The Journal of the Astronautical Sciences (2018) 65: 423–447
https://doi.org/10.1007/s40295-018-0133-0

Spacecraft Dynamics Employing a General Multi-tank and Multi-thruster Mass Depletion Formulation

Paolo Panicucci[1,4] · **Cody Allard**[2] · **Hanspeter Schaub**[3]

Published online: 24 October 2018

Abstract

Using thrusters for either orbital maneuvers or attitude control change the current spacecraft mass properties and results in an associated reaction force and torque. To perform orbital and attitude control using thrusters, or to obtain optimal trajectories, the impact of mass variation and depletion of the spacecraft must be thoroughly understood. Some earlier works make rocket-body specific assumptions such as axial symmetric bodies or certain tank geometries hat limit the applicability of the models. Other earlier works require further derivation to implement the provided equations of motion in simulation software. This paper develops the fully coupled translational and rotational equations of motion of a spacecraft that is ejecting mass through the use of thrusters and can be readily implemented in flight dynamics software. The derivation begins considering the entire closed system: the spacecraft and the ejected fuel. Then the exhausted fuel motion in free space is expressed using the thruster nozzle properties and the familiar thrust vector to avoid tracking the expelled fuel in the simulation. Additionally, the present formulation considers a general multi-tank and multi-thruster approach to account for both the depleting fuel mass in the tanks and the mass exiting the thruster nozzles. General spacecraft configurations are possible where thrusters can pull from a single tank or multiple tanks, and the tank being drawn from can be switched via a valve. Numerical simulations are presented to perform validation of the model developed and to show the impact of assumptions that are made for mass depletion in prior developed models.

✉ Paolo Panicucci
paolo.panicucci@isae-supaero.fr

[1] Dipartimento di Ingegneria Aerospaziale ed Astronautica, University of Roma “La Sapienza”, Roma, Italy

[2] Aerospace Engineering Sciences, University of Colorado Boulder, Boulder, CO 80309, USA

[3] Glenn L. Murphy Chair of Engineering, Department of Aerospace Engineering Sciences, AAS Fellow, University of Colorado, 431 UCB, Colorado Center for Astrodynamics Research, Boulder, CO 80309-0431, USA

[4] Present address: Institut Supérieur de l’Aéronautique et de l’Espace - SUPAERO, 10 Avenue Edouard Belin, 31400, Toulouse, France

Keywords Variable mass systems · Equations of motion · Spacecraft dynamics

Introduction

The aerospace industry has been steadily increasing the accuracy of spacecraft simulations using advanced analytical development and computer numerical techniques. The prediction of satellite behaviors and their orbits during the preliminary design phase and leading up to the operational period is an extremely useful tool to develop and analyze missions. Moreover, high-fidelity models provide an efficient way to limit fuel demanding maneuvers to preserve satellite orbital position. In this context, the need of a general formulation to predict satellite orbital and attitude behaviors while considering mass depletion is crucial to model the dynamical mass variation influence on the equations of motion (EOMs). The simplest way to take into account the ejection of propellant is to use an "update-only" approach [1], thus updating the center of mass position and the inertia during the simulation in the EOMs without considering the dynamical influences of the mass depletion. This results in an easy-to-implement model whose limitations consist in the lack of detailed attitude and translational motion prediction for high-fidelity purposes. A more accurate approach considers the spacecraft as an open system whose mass changes in accord with the fuel flows. Pioneering work in Reference [2] about this subject derives the EOMs by considering a system of particles. In contrast, prior works [3, 4] introduce the problem as a continuous system by using the Reynolds transport theorem with an integral notation. References [5–9] present the derivation of a variable mass rocket with an axial-symmetric design with a single axial-symmetric burn chamber and a circular nozzle in order to take into account observed experimental results from flight campaigns [10, 11]. These assumptions decouple the rocket axial spin from the transverse angular velocity and results in a closed solution to the problem, however, the assumptions limit the application to axial symmetric spacecraft. References [12] and [13] present the EOMs considering a system of coaxial bodies with different angular velocities. The studies present an analysis of the nutation angle in the case of a two-body satellite, like a spacecraft with a coaxial wheel. The equations must be specified accordingly with the number of interconnected bodies and this results in the need of re-derivation for a specific system of interconnected bodies and to take into account how particles leave the system. A more recent work [14] considers a body fixed reference origin and develops the translational and rotational EOM for a reentry module. The EOMs, although general, are presented in integral form. Therefore, the EOMs require further derivation to be implemented into simulation software. Additionally, the model lacks in a defined approach to connect the dynamical spacecraft mass properties variation with the ejected mass characteristics.

In contrast to the literature, this research sets out to develop the EOMs for a spacecraft that is ejecting fuel through the use of thrusters without making assumptions involving the spacecraft geometry, tank geometry, or the complexity of the propulsive system. More specifically, this paper provides the detailed analytical formulation of this problem, is applicable to a wide variety of spacecraft and can be readily implemented in simulation software without excessive coding efforts or re-derivation of

EOMs. The formulation itself is intended to be thorough and methodical to answer this complex problem. Additionally, this research is focused on the formalization of a general multi-tank and multi-thruster approach to link the mass depletion inside the tanks with the fuel ejected by the nozzles and the resulting impact on the orbital and attitude motion. Variations on the type of tank or thruster models can be implemented in the presented model without increased model complexity as the gathering of the EOMs is general. Furthermore, the model is derived to be as modular as possible to be easily implemented in flight dynamics software.

Problem Statement

To help define the problem, Fig. 1 is displayed. This problem involves a spacecraft consisting of a hub which is a rigid body and has a center of mass location labeled as point Bc. The hub has M number of tanks and N number of thrusters attached to it. The figure only shows one tank and one thruster but the analytical development is general. The i_{th} tank has a center of mass location labeled as Fc_i and the j_{th} thruster is located at Nc_j. The body fixed reference frame $\mathcal{B}$: $\{\hat{\boldsymbol{b}}_1\,, \hat{\boldsymbol{b}}_2\,, \hat{\boldsymbol{b}}_3\}$ with origin B can be oriented in any direction and point B can be located anywhere fixed to the hub. This means that point B and the center of mass location of the spacecraft, C, are not necessarily coincident. As a result, the vector $\boldsymbol{c}$ defines the vector pointing from the body frame origin to the center of mass fo the spacecraft. The inertial reference frame $\mathcal{N}$: $\{\hat{\boldsymbol{n}}_1\,, \hat{\boldsymbol{n}}_2\,, \hat{\boldsymbol{n}}_3\}$ is centered at N and is fixed in inertial space.

Another important description of this problem are the assumptions being used. The following list organizes the assumptions that are used for this formulation:

- The spacecraft hub is rigid and deformations are not considered.

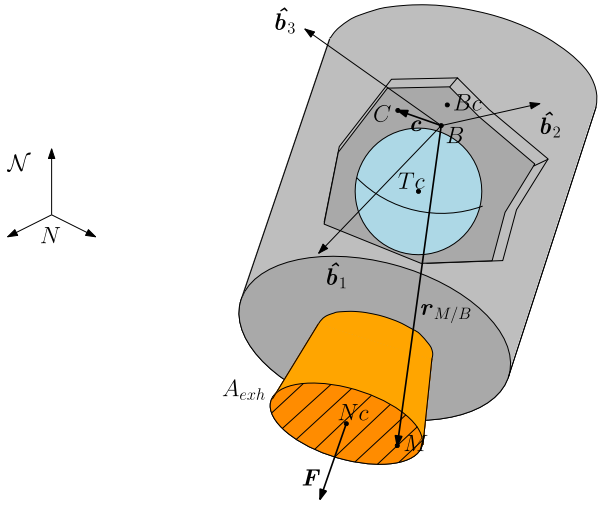

Fig. 1 Spacecraft with depleting mass and definition of frames and variables

- The mass flow among the tanks, the thrusters and in the combustion chamber are considered to be second order effects and neglected. As a consequence fluid motions in pipeline and pumps, and gas whirling are not taken into account. However, the fuel expenditure related time varying fuel tank mass properties, such as total mass and inertia, are taking into account.
- The relative motion between the propellant and the fuel tanks, such as fuel sloshing, is not considered in this present work
- The particles are accelerated instantaneously from the spacecraft velocity $\dot{\boldsymbol{r}}_{B/N}$ to the exhausted velocity $\boldsymbol{v}_{\text{exh}}$ at the nozzle exit.
- The particle exhausted velocity $\boldsymbol{v}_{\text{exh}}$ is considered constant and parallel to the nozzle's normal $\hat{\boldsymbol{n}}$.

Throughout this paper, vector calculus is used and the notation to define certain quantities needs to be introduced. A position vector, $\boldsymbol{r}_{C/N}$, is the vector pointing from N to C. $\boldsymbol{\omega}_{\mathcal{B}/\mathcal{N}}$ is the angular velocity of the $\mathcal{B}$ frame with respect to the $\mathcal{N}$ frame. $\dot{\boldsymbol{r}}$ denotes an inertial time derivate of vector $\boldsymbol{r}$ and $\boldsymbol{r}'$ defines a time derivate of $\boldsymbol{r}$ with respect to the body frame. Using these definitions, the following section develops the EOMs for the spacecraft system.

Equations of Motion

Reynolds Transport Theorem and Continuity Equation

In this section the main tool used for the development of the governing equations is presented and explained. The Reynolds transport theorem provides a basic tool to pass from a Lagrangian formulation, based on the analysis of particles moving in space, to an Eulerian one, which considers a fixed space volume where physical quantities are exchanged through the boundaries.

In the present document, the Lagrangian system is labeled *Body*, the moving volume of the Eulerian approach is labeled $\mathcal{V}_{\text{sc}}$ and its surface $\mathcal{A}_{\text{sc}}$ are represented in Fig. 2.

By using this notation, the Reynolds transport theorem affirms [3, 15–17]:

$$\frac{^{\mathcal{D}}\mathrm{d}}{\mathrm{d}t}\int_{\text{Body}}\rho\,\boldsymbol{f}\,\mathrm{d}\mathcal{V}=\frac{^{\mathcal{D}}\mathrm{d}}{\mathrm{d}\,t}\int_{\mathcal{V}_{\text{sc}}}\rho\,\boldsymbol{f}\,\mathrm{d}\mathcal{V}+\int_{\mathcal{A}_{\text{sc}}}\rho\,\boldsymbol{f}\left(\boldsymbol{v}_{\text{rel}}\cdot\hat{\boldsymbol{n}}\right)\mathrm{d}A \tag{1}$$

where $\boldsymbol{f}$ is a general vectorial quantity transported out from the control volume, ρ is the density of the infinitesimal mass $\mathrm{d}m$, $\hat{\boldsymbol{n}}$ the surface normal considered positive if exiting from the control volume, $\mathcal{D}$ is a generic reference frame and $\boldsymbol{v}_{\text{rel}}$ is the relative velocity of the particles flowing out from the surface with respect to the control surface itself. This last quantity can be easily defined as $\boldsymbol{v}_{\text{rel}}(\boldsymbol{x},t)=\frac{^{\mathcal{D}}\mathrm{d}}{\mathrm{d}t}\boldsymbol{r}_{M/B}(\boldsymbol{x},t)-\boldsymbol{v}_{\text{surf}}(\boldsymbol{x},t)$ where $\frac{^{\mathcal{D}}\mathrm{d}}{\mathrm{d}t}\boldsymbol{r}_{M/B}(\boldsymbol{x},t)$ is the particles' velocity with respect to the $\mathcal{D}$ frame and $\boldsymbol{v}_{\text{surf}}(\boldsymbol{x},t)$ is the control surface velocity with respect to the $\mathcal{D}$ reference frame.

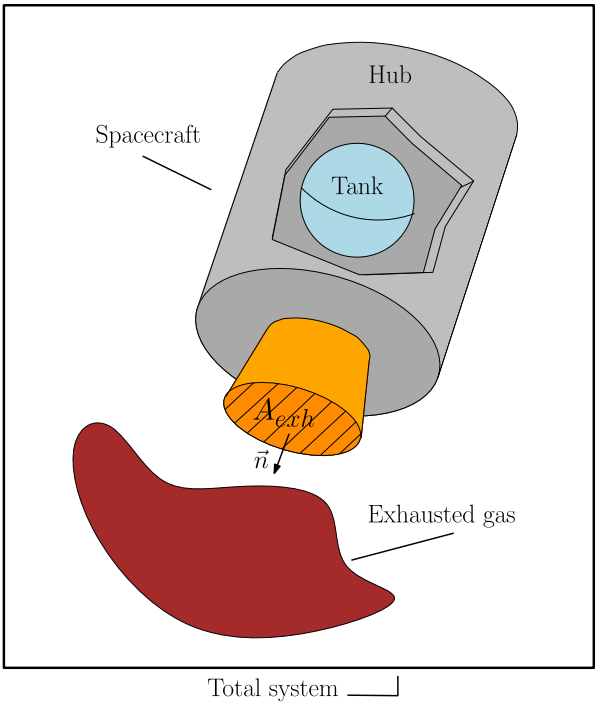

Fig. 2 Division of the total system in spacecraft and exhausted gas. The control surface $\mathcal{A}_{\text{sc}}$ represents the exchanging surface between the two subsystems

Moreover, if the control volume is fixed in the $\mathcal{D}$ frame and no deformable control volume is considered, the following relation is proved [14, 16]:

$$\frac{^{\mathcal{D}}\mathrm{d}}{\mathrm{d}t}\int_{\text{Body}}\rho\,\boldsymbol{f}\,\mathrm{d}\mathcal{V}=\int_{\mathcal{V}_{\text{sc}}}\frac{^{\mathcal{D}}\partial}{\partial t}\left(\rho\,\boldsymbol{f}\right)\mathrm{d}\mathcal{V}+\int_{\mathcal{A}_{\text{sc}}}\rho\,\boldsymbol{f}\left(\frac{^{\mathcal{D}}\mathrm{d}}{\mathrm{d}t}\boldsymbol{r}_{M/B}\right)\cdot\hat{\boldsymbol{n}}\,\mathrm{d}A \tag{2}$$

An additional key equation that is used throughout the paper is the continuity equation. First, the continuity equation is gathered:

$$\frac{\mathrm{d}}{\mathrm{d}t}\int_{\text{Body}}\mathrm{d}m=\frac{\mathrm{d}}{\mathrm{d}t}\int_{\mathcal{V}_{\text{sc}}}\rho\,\mathrm{d}\mathcal{V}+\int_{\mathcal{A}_{\text{sc}}}\rho\,\boldsymbol{v}_{\text{rel}}\cdot\hat{\boldsymbol{n}}\,\mathrm{d}\mathcal{A}=0 \tag{3}$$

The rate of change of the spacecraft is defined as $\dot{m}_{\text{sc}}=\dfrac{\mathrm{d}}{\mathrm{d}t}\displaystyle\int_{\mathcal{V}_{\text{sc}}}\rho\,\mathrm{d}\mathcal{V}$ and yields:

$$\dot{m}_{\text{sc}}=-\int_{\mathcal{A}_{\text{sc}}}\rho\,\boldsymbol{v}_{\text{rel}}\cdot\hat{\boldsymbol{n}}\,\mathrm{d}\mathcal{A}\qquad\Rightarrow\qquad\mathrm{d}\dot{m}=-\rho\,\boldsymbol{v}_{\text{rel}}\cdot\hat{\boldsymbol{n}}\,\mathrm{d}\mathcal{A} \tag{4}$$

This definition will be used in the derivation of the EOMs.

Translational Equation of Motion

The derivation of the translational EOM begins considering Newton's law for a closed system

$$\frac{{}^{\mathcal{N}}\mathrm{d}}{\mathrm{d}t}\int_{\mathrm{Body}} \dot{\boldsymbol{r}}_{M/N}\,\mathrm{d}m = \boldsymbol{F}_{\mathrm{ext}} \tag{5}$$

where $\dot{\boldsymbol{r}}_{M/N}$ is the velocity of a particle at the M point expressed with respect to the inertial reference frame and $\boldsymbol{F}_{\mathrm{ext}}$ is the sum of the external forces experienced by the body. As the total mass of the system is constant, the differentiation operator is brought inside the integration:

$$\frac{{}^{\mathcal{N}}\mathrm{d}}{\mathrm{d}t}\int_{\mathrm{Body}} \dot{\boldsymbol{r}}_{M/N}\,\mathrm{d}m = \int_{\mathrm{Body}} \ddot{\boldsymbol{r}}_{M/N}\,\mathrm{d}m \tag{6}$$

The acceleration of the origin of the $\mathcal{B}$ frame is expressed as $\ddot{\boldsymbol{r}}_{M/N} = \ddot{\boldsymbol{r}}_{B/N} + \ddot{\boldsymbol{r}}_{M/B}$. By using the kinematic transport theorem, the expression of $\ddot{\boldsymbol{r}}_{M/B}$ is found:

$$\dot{\boldsymbol{r}}_{M/B} = \boldsymbol{r}'_{M/B} + \boldsymbol{\omega}_{\mathcal{B}/\mathcal{N}} \times \boldsymbol{r}_{M/B} \tag{7}$$

$$\ddot{\boldsymbol{r}}_{M/B} = \boldsymbol{r}''_{M/B} + 2\,\boldsymbol{\omega}_{\mathcal{B}/\mathcal{N}} \times \boldsymbol{r}'_{M/B} + \dot{\boldsymbol{\omega}}_{\mathcal{B}/\mathcal{N}} \times \boldsymbol{r}_{M/B} + \boldsymbol{\omega}_{\mathcal{B}/\mathcal{N}} \times \left(\boldsymbol{\omega}_{\mathcal{B}/\mathcal{N}} \times \boldsymbol{r}_{B/M}\right) \tag{8}$$

A Lagrangian formulation of linear momentum is deduced by using Eqs. 5, 6 and 8:

$$\int_{\mathrm{Body}} \left(\ddot{\boldsymbol{r}}_{B/N} + \dot{\boldsymbol{\omega}}_{\mathcal{B}/\mathcal{N}} \times \boldsymbol{r}_{M/B} + \boldsymbol{\omega}_{\mathcal{B}/\mathcal{N}} \times \left(\boldsymbol{\omega}_{\mathcal{B}/\mathcal{N}} \times \boldsymbol{r}_{M/B}\right)\right) \mathrm{d}m + 2\,\boldsymbol{\omega}_{\mathcal{B}/\mathcal{N}} \times \int_{\mathrm{Body}} \boldsymbol{r}'_{M/B}\mathrm{d}m + \int_{\mathrm{Body}} \boldsymbol{r}''_{M/B}\mathrm{d}m = \boldsymbol{F}_{\mathrm{ext}} \tag{9}$$

The system mass is constant, therefore the derivative operator can be applied after the integration yielding

$$\int_{\mathrm{Body}} \boldsymbol{r}'_{M/B}\mathrm{d}m = \frac{{}^{\mathcal{B}}\mathrm{d}}{\mathrm{d}t}\int_{\mathrm{Body}} \boldsymbol{r}_{M/B}\mathrm{d}m \tag{10}$$

$$\int_{\mathrm{Body}} \boldsymbol{r}''_{M/B}\mathrm{d}m = \frac{{}^{\mathcal{B}}\mathrm{d}^2}{\mathrm{d}t^2}\int_{\mathrm{Body}} \boldsymbol{r}_{M/B}\mathrm{d}m \tag{11}$$

By using the Reynolds transport theorem, Eqs. 10 and 11 are expressed in a space fixed volume, shown in Fig. 2. Performing this conversion results in the following equations:

$$\frac{{}^{\mathcal{B}}\mathrm{d}}{\mathrm{d}t}\int_{\mathrm{Body}} \boldsymbol{r}_{M/B}\,\mathrm{d}m = \frac{{}^{\mathcal{B}}\mathrm{d}}{\mathrm{d}t}\int_{\mathcal{V}_{\mathrm{sc}}} \rho\,\boldsymbol{r}_{M/B}\,\mathrm{d}\mathcal{V} + \int_{\mathcal{A}_{\mathrm{sc}}} \rho\,\boldsymbol{r}'_{M/B}\cdot\hat{\boldsymbol{n}}\,\boldsymbol{r}_{M/B}\mathrm{d}A \tag{12}$$

$$\frac{{}^{\mathcal{B}}\mathrm{d}^2}{\mathrm{d}t^2}\int_{\mathrm{Body}} \boldsymbol{r}_{M/B}\,\mathrm{d}m = \frac{{}^{\mathcal{B}}\mathrm{d}^2}{\mathrm{d}t^2}\int_{\mathcal{V}_{\mathrm{sc}}} \rho\,\boldsymbol{r}_{M/B}\,\mathrm{d}\mathcal{V} + \frac{{}^{\mathcal{B}}\mathrm{d}}{\mathrm{d}t}\int_{\mathcal{A}_{\mathrm{sc}}} \rho\,\boldsymbol{r}'_{M/B}\cdot\hat{\boldsymbol{n}}\,\boldsymbol{r}_{M/B}\,\mathrm{d}A + \int_{\mathcal{A}_{\mathrm{sc}}} \rho\,\boldsymbol{r}'_{M/B}\cdot\hat{\boldsymbol{n}}\,\boldsymbol{r}'_{M/B}\,\mathrm{d}A \tag{13}$$

where $\boldsymbol{v}_{\text{rel}} = \boldsymbol{r}'_{M/B}$ because point B is fixed with respect to the spacecraft. Equation 9 is re-organized by using the previous relations in order to consider an Eulerian approach, i.e. based on a volume-based derivation:

$$\begin{aligned}\int_{\text{Body}} \left(\ddot{\boldsymbol{r}}_{B/N} + \dot{\boldsymbol{\omega}}_{\mathcal{B}/\mathcal{N}} \times \boldsymbol{r}_{M/B} + \boldsymbol{\omega}_{\mathcal{B}/\mathcal{N}} \times \left(\boldsymbol{\omega}_{\mathcal{B}/\mathcal{N}} \times \boldsymbol{r}_{M/B}\right)\right) \mathrm{d}m \\ + 2\,\boldsymbol{\omega}_{\mathcal{B}/\mathcal{N}} \times \left(\frac{{}^{\mathcal{B}}\mathrm{d}}{\mathrm{d}t} \int_{\mathcal{V}_{\text{sc}}} \rho\, \boldsymbol{r}_{M/B}\, \mathrm{d}\mathcal{V} + \int_{\mathcal{A}_{\text{sc}}} \rho\, \boldsymbol{r}'_{M/B} \cdot \hat{\boldsymbol{n}}\, \boldsymbol{r}_{M/B} \mathrm{d}A \right) \\ + \frac{{}^{\mathcal{B}}\mathrm{d}^2}{\mathrm{d}t^2} \int_{\mathcal{V}_{\text{sc}}} \rho\, \boldsymbol{r}_{M/B}\, \mathrm{d}\mathcal{V} \\ + \frac{{}^{\mathcal{B}}\mathrm{d}}{\mathrm{d}t} \int_{\mathcal{A}_{\text{sc}}} \rho\, \boldsymbol{r}'_{M/B} \cdot \hat{\boldsymbol{n}}\, \boldsymbol{r}_{M/B}\, \mathrm{d}A + \int_{\mathcal{A}_{\text{sc}}} \rho\, \boldsymbol{r}'_{M/B} \cdot \hat{\boldsymbol{n}}\, \boldsymbol{r}'_{M/B}\, \mathrm{d}A = \boldsymbol{F}_{\text{ext}} \end{aligned} \tag{14}$$

As explained in previous work [15], if all of the mass is contained in the control volume at the initial time, then a particular relation results because no mass is outside the control volume at $t = 0$ and the dynamic quantities will be transported out during the integration. This relationship is quantified in the following equation:

$$\begin{aligned}\boldsymbol{F}_{\text{ext}} - \int_{\text{Body}} \left(\ddot{\boldsymbol{r}}_{B/N} + \dot{\boldsymbol{\omega}}_{\mathcal{B}/\mathcal{N}} \times \boldsymbol{r}_{M/B} + \boldsymbol{\omega}_{\mathcal{B}/\mathcal{N}} \times \left(\boldsymbol{\omega}_{\mathcal{B}/\mathcal{N}} \times \boldsymbol{r}_{M/B}\right)\right) \mathrm{d}m = \int_{\mathcal{V}_{\text{sc}}} \mathrm{d}\boldsymbol{F}_{\text{vol}} \\ + \int_{\mathcal{A}_{\text{sc}}} \mathrm{d}\boldsymbol{F}_{\text{surf}} - \int_{\mathcal{V}_{\text{sc}}} \rho \left(\ddot{\boldsymbol{r}}_{B/N} + \dot{\boldsymbol{\omega}}_{\mathcal{B}/\mathcal{N}} \times \boldsymbol{r}_{M/B} + \boldsymbol{\omega}_{\mathcal{B}/\mathcal{N}} \times \left(\boldsymbol{\omega}_{\mathcal{B}/\mathcal{N}} \times \boldsymbol{r}_{M/B}\right)\right) \mathrm{d}\mathcal{V} \end{aligned} \tag{15}$$

where the forces are divided into volumetric forces and the forces applied on the spacecraft surface. Rearranging this result, replacing the definition of $\boldsymbol{F}_{\text{ext}}$, and isolating the forces to the right hand side of the equation yields:

$$\begin{aligned}\int_{\mathcal{V}_{\text{sc}}} \rho \left(\ddot{\boldsymbol{r}}_{B/N} + \dot{\boldsymbol{\omega}}_{\mathcal{B}/\mathcal{N}} \times \boldsymbol{r}_{M/B} + \boldsymbol{\omega}_{\mathcal{B}/\mathcal{N}} \times \left(\boldsymbol{\omega}_{\mathcal{B}/\mathcal{N}} \times \boldsymbol{r}_{M/B}\right)\right) \mathrm{d}\mathcal{V} \\ + 2\,\boldsymbol{\omega}_{\mathcal{B}/\mathcal{N}} \times \left(\frac{{}^{\mathcal{B}}\mathrm{d}}{\mathrm{d}t} \int_{\mathcal{V}_{\text{sc}}} \rho\, \boldsymbol{r}_{M/B}\, \mathrm{d}\mathcal{V} + \int_{\mathcal{A}_{\text{sc}}} \rho\, \boldsymbol{r}'_{M/B} \cdot \hat{\boldsymbol{n}}\, \boldsymbol{r}_{M/B} \mathrm{d}A \right) \\ + \frac{{}^{\mathcal{B}}\mathrm{d}^2}{\mathrm{d}t^2} \int_{\mathcal{V}_{\text{sc}}} \rho\, \boldsymbol{r}_{M/B}\, \mathrm{d}\mathcal{V} \\ + \frac{{}^{\mathcal{B}}\mathrm{d}}{\mathrm{d}t} \int_{\mathcal{A}_{\text{sc}}} \rho\, \boldsymbol{r}'_{M/B} \cdot \hat{\boldsymbol{n}}\, \boldsymbol{r}_{M/B}\, \mathrm{d}A + \int_{\mathcal{A}_{\text{sc}}} \rho\, \boldsymbol{r}'_{M/B} \cdot \hat{\boldsymbol{n}}\, \boldsymbol{r}'_{M/B}\, \mathrm{d}A = \int_{\mathcal{V}_{\text{sc}}} \mathrm{d}\boldsymbol{F}_{\text{vol}} \\ + \int_{\mathcal{A}_{\text{sc}}} \mathrm{d}\boldsymbol{F}_{\text{surf}} \end{aligned} \tag{16}$$

One goal for this paper is to develop the EOMs of a spacecraft with depleting mass without the necessity of continuing to track the depleted mass once it has left the spacecraft. One aspect of achieving this goal, is to define the center of mass of the

spacecraft with respect to point B, including the remaining fuel while disregarding the spent fuel. This variable, $\boldsymbol{c} = \boldsymbol{r}_{C/B}$, is defined as:

$$\boldsymbol{c} = \frac{m_{\text{hub}}\,\boldsymbol{r}_{Bc/B} + \sum_{i=1}^{M} m_{\text{fuel}_i}\,\boldsymbol{r}_{Fc_i/B}}{m_{\text{hub}} + \sum_{i=1}^{M} m_{\text{fuel}_i}} \tag{17}$$

where m_{hub} is the mass of the hub, m_{fuel_i} is the i^{th} tank's fuel mass and $\boldsymbol{r}_{Fc_i/B}$ is the position of the center of mass of the i^{th} tank.

In order to infer the influence of the mass variation in the EOMs the first and second time derivatives with respect to the body frame of $\boldsymbol{c}$ are defined:

$$\begin{aligned}\boldsymbol{c}' = &\frac{\sum_{i=1}^{M}\left(\dot{m}_{\text{fuel}_i}\boldsymbol{r}_{Fc_i/B} + m_{\text{fuel}_i}\boldsymbol{r}'_{Fc_i/B}\right)}{m_{\text{hub}} + \sum_{i=1}^{M} m_{\text{fuel}_i}} \\ &- \frac{\left(\sum_{i=1}^{M}\dot{m}_{\text{fuel}_i}\right)\left(m_{\text{hub}}\,\boldsymbol{r}_{Bc/B} + \sum_{i=1}^{M} m_{\text{fuel}_i}\,\boldsymbol{r}_{Fc_i/B}\right)}{\left(m_{\text{hub}} + \sum_{i=1}^{M} m_{\text{fuel}_i}\right)^2}\end{aligned} \tag{18}$$

$$\begin{aligned}\boldsymbol{c}'' = &\frac{\sum_{i=1}^{M}\left(\ddot{m}_{\text{fuel}_i}\boldsymbol{r}_{Fc_i/B} + 2\,\dot{m}_{\text{fuel}_i}\boldsymbol{r}'_{Fc_i/B} + m_{\text{fuel}_i}\boldsymbol{r}''_{Fc_i/B}\right)}{m_{\text{hub}} + \sum_{i=1}^{M} m_{\text{fuel}_i}} \\ &- \frac{\left(\sum_{i=1}^{M}\ddot{m}_{\text{fuel}_i}\right)\left(m_{\text{hub}}\,\boldsymbol{r}_{Bc/B} + \sum_{i=1}^{M} m_{\text{fuel}_i}\,\boldsymbol{r}_{Fc_i/B}\right)}{\left(m_{\text{hub}} + \sum_{i=1}^{M} m_{\text{fuel}_i}\right)^2} \\ &- \frac{2\left(\sum_{i=1}^{M}\dot{m}_{\text{fuel}_i}\right)\sum_{i=1}^{M}\left(\dot{m}_{\text{fuel}_i}\boldsymbol{r}_{Fc_i/B} + m_{\text{fuel}_i}\boldsymbol{r}'_{Fc_i/B}\right)}{\left(m_{\text{hub}} + \sum_{i=1}^{M} m_{\text{fuel}_i}\right)^2} \\ &+ \frac{2\left(\sum_{i=1}^{M}\dot{m}_{\text{fuel}_i}\right)^2\left(m_{\text{hub}}\boldsymbol{r}_{Bc/B} + \sum_{i=1}^{M} m_{\text{fuel}_i}\boldsymbol{r}_{Fc_i/B}\right)}{\left(m_{\text{hub}} + \sum_{i=1}^{M} m_{\text{fuel}_i}\right)^3}\end{aligned} \tag{19}$$

Using these definitions of $\boldsymbol{c}$ and its derivatives, the translational EOM can be simplified. Additionally, some assumptions need to be defined to further simplify the translational EOM. The hub is assumed to be rigid, therefore deformations are not considered. The mass flow within the tanks and the thrusters is assumed to be a second order effect and ignored for this paper. The particles are assumed to be accelerated instantaneously from the spacecraft velocity, $\dot{\boldsymbol{r}}_{B/N}$, to the exhausted velocity $\boldsymbol{v}_{\text{exh}}$ at the nozzle. And the exhausted velocity $\boldsymbol{v}_{\text{exh}}$ is considered constant and parallel to the nozzle's normal $\hat{\boldsymbol{n}}$.

The first integral in Eq. 16 is computed using the fact that $\boldsymbol{r}_{M/B} = \boldsymbol{c} + \boldsymbol{r}_{M/C}$ and the result is shown in the following equation:

$$\begin{aligned}\int_{\mathcal{V}_{\text{sc}}} \rho\,\left(\ddot{\boldsymbol{r}}_{B/N} + \dot{\boldsymbol{\omega}}_{\mathcal{B}/\mathcal{N}} \times \boldsymbol{r}_{M/B} + \boldsymbol{\omega}_{\mathcal{B}/\mathcal{N}} \times \left(\boldsymbol{\omega}_{\mathcal{B}/\mathcal{N}} \times \boldsymbol{r}_{M/B}\right)\right) \mathrm{d}\mathcal{V} = m_{\text{sc}}\,\ddot{\boldsymbol{r}}_{B/N} \\ + m_{\text{sc}}\,\dot{\boldsymbol{\omega}}_{\mathcal{B}/\mathcal{N}} \times \boldsymbol{c} + m_{\text{sc}}\,\boldsymbol{\omega}_{\mathcal{B}/\mathcal{N}} \times \left(\boldsymbol{\omega}_{\mathcal{B}/\mathcal{N}} \times \boldsymbol{c}\right)\end{aligned} \tag{20}$$

where $m_{\text{sc}} = m_{\text{hub}} + \sum_{i=1}^{M} m_{\text{fuel}_i}$ is the instantaneous mass of the spacecraft. The second and fourth integrals are computed and yield:

$$\frac{\mathcal{B}\mathrm{d}}{\mathrm{d}t}\int_{\mathcal{V}_{\text{sc}}} \rho\, \boldsymbol{r}_{M/B}\,\mathrm{d}\mathcal{V} = \frac{\mathcal{B}\mathrm{d}}{\mathrm{d}t}\left(m_{\text{sc}}\,\boldsymbol{c}\right) = m_{\text{sc}}\,\boldsymbol{c}' + \dot{m}_{\text{fuel}}\boldsymbol{c} \tag{21}$$

$$\frac{\mathcal{B}\mathrm{d}^2}{\mathrm{d}t^2}\int_{\mathcal{V}_{\text{sc}}} \rho\, \boldsymbol{r}_{M/B}\,\mathrm{d}\mathcal{V} = \frac{\mathcal{B}\mathrm{d}^2}{\mathrm{d}t^2}\left(m_{\text{sc}}\,\boldsymbol{c}\right) = m_{\text{sc}}\,\boldsymbol{c}'' + 2\,\dot{m}_{\text{fuel}}\,\boldsymbol{c}' + \ddot{m}_{\text{fuel}}\boldsymbol{c} \tag{22}$$

where $\dot{m}_{\text{fuel}} = \sum_{i=1}^{M}\dot{m}_{\text{fuel}_i}$ and $\ddot{m}_{\text{fuel}} = \sum_{i=1}^{M}\ddot{m}_{\text{fuel}_i}$.

In order to find the terms calculated on the reference surface seen in the third, fifth and sixth integrals, it is convenient to separate the integrals on the surface of each nozzle. Moreover, as the fuel's properties are flowing out of a surface plane, it is convenient to consider that $\boldsymbol{r}_{M/B} = \boldsymbol{r}_{M/Nc_j} + \boldsymbol{r}_{Nc_j/B}$ where Nc_i is the area's geometric center. Finally, an appropriate variable transformation is given in Eq. 4. Performing these calculations on the third integral results in:

$$\int_{\mathcal{A}_{\text{sc}}} \rho\, \boldsymbol{r}'_{M/B}\cdot\hat{\boldsymbol{n}}\,\boldsymbol{r}_{M/B}\,\mathrm{d}A = -\sum_{j=1}^{N}\int_{\dot{m}_{\text{noz}_j}}\left(\boldsymbol{r}_{M/Nc_j} + \boldsymbol{r}_{Nc_j/B}\right)\mathrm{d}\dot{m} = -\sum_{j=1}^{N}\dot{m}_{\text{noz}_j}\boldsymbol{r}_{Nc_j/B} \tag{23}$$

where the first part of the integral is null because of barycenter definition and $\dot{m}_{\text{noz}_j}$ is the mass flow of the j^{th} nozzle. The fifth integral in Eq. 16 yields:

$$\frac{\mathcal{B}\mathrm{d}}{\mathrm{d}t}\int_{\mathcal{A}_{\text{sc}}} \rho\, \boldsymbol{r}'_{M/B}\cdot\hat{\boldsymbol{n}}\,\boldsymbol{r}_{M/B}\,\mathrm{d}A = \frac{\mathcal{B}\mathrm{d}}{\mathrm{d}t}\left(-\sum_{j=1}^{N}\dot{m}_{\text{noz}_j}\boldsymbol{r}_{Nc_j/B}\right) = -\sum_{j=1}^{N}\ddot{m}_{\text{noz}_j}\boldsymbol{r}_{Nc_j/B} \tag{24}$$

Using the assumption introduced earlier in this section, $\boldsymbol{r}'_{M/B} = \boldsymbol{v}_{\text{exh}}$, the sixth is integral is found and can be in the following equation:

$$\int_{\mathcal{A}_{\text{sc}}} \rho\, \boldsymbol{r}'_{M/B}\cdot\hat{\boldsymbol{n}}\,\boldsymbol{r}'_{M/B}\,\mathrm{d}A = \sum_{j=1}^{N}\int_{\mathcal{A}_{\text{noz}_j}} \rho\, \boldsymbol{r}'_{M/B}\cdot\boldsymbol{n}\,\boldsymbol{r}'_{M/B}\mathrm{d}A = -\sum_{j=1}^{N}\dot{m}_{\text{noz}_j}\,\boldsymbol{v}_{\text{exh}_j} \tag{25}$$

where $\boldsymbol{v}_{\text{exh}_j}$ is the exhausted velocity of a particle exiting from the j^{th} nozzle.

The two integrals on the right-hand-side of Eq. 16 depends on the force model chosen. Therefore, to not lose generality, the resulting surface integral due to the pressure jump between the nozzle and the environment is the only term that is analytically computed seen in the following equation:

$$\int_{\mathcal{V}_{\text{sc}}}\mathrm{d}\boldsymbol{F}_{\text{vol}} + \int_{\mathcal{A}_{\text{sc}}}\mathrm{d}\boldsymbol{F}_{\text{surf}} = \boldsymbol{F}_{\text{ext, vol}} + \boldsymbol{F}_{\text{ext, surf}} + \sum_{j=1}^{N}\frac{\boldsymbol{v}_{\text{exh}_j}}{v_{\text{exh}_j}}\,A_{\text{noz}_j}\left(p_{\text{exh}_j} - p_{\text{atm}}\right) \tag{26}$$

where $\boldsymbol{F}_{\text{ext, vol}}$ are the external forces acting on the control volume, $\boldsymbol{F}_{\text{ext, surf}}$ are the external forces accelerating the control surface, p_{exh_j} is the particles' exhausted pressure at the j^{th} nozzle and p_{atm} is the atmospheric pressure at the flying altitude.

Finally, Eq. 16 is rewritten considering the nozzles' geometry and fluid properties by using Eqs. 21–26:

$$\begin{aligned} m_{\mathrm{sc}}\ddot{\boldsymbol{r}}_{B/N} &+ m_{\mathrm{sc}}\,\dot{\boldsymbol{\omega}}_{\mathcal{B}/\mathcal{N}} \times \boldsymbol{c} + m_{\mathrm{sc}}\,\boldsymbol{\omega}_{\mathcal{B}/\mathcal{N}} \times \left(\boldsymbol{\omega}_{\mathcal{B}/\mathcal{N}} \times \boldsymbol{c}\right) + m_{\mathrm{sc}}\,\boldsymbol{c}'' + 2\,\dot{m}_{\mathrm{fuel}}\,\boldsymbol{c}' \\ &+ \ddot{m}_{\mathrm{fuel}}\boldsymbol{c} + 2\,\boldsymbol{\omega}_{\mathcal{B}/\mathcal{N}} \times \left(m_{\mathrm{sc}}\,\boldsymbol{c}' + \dot{m}_{\mathrm{fuel}}\boldsymbol{c} - \sum_{j=1}^{N} \dot{m}_{\mathrm{noz}_j}\boldsymbol{r}_{Nc_j/B}\right) \\ &- \sum_{j=1}^{N} \ddot{m}_{\mathrm{noz}_j}\boldsymbol{r}_{Nc_j/B} - \sum_{j=1}^{N} \dot{m}_{\mathrm{noz}_j}\,\boldsymbol{v}_{\mathrm{exh}_j} = \boldsymbol{F}_{\mathrm{ext,\,vol}} + \boldsymbol{F}_{\mathrm{ext,\,surf}} \\ &+ \sum_{j=1}^{N} \frac{\boldsymbol{v}_{\mathrm{exh}_j}}{v_{\mathrm{exh}_j}}\,A_{\mathrm{noz}_j}\left(p_{\mathrm{exh}_j} - p_{\mathrm{atm}}\right) \end{aligned} \tag{27}$$

The above development is simplified by introducing the classical thruster force to fuel mass rate relation:

$$\boldsymbol{F}_{\mathrm{thr}_j} = \boldsymbol{v}_{\mathrm{exh}_j}\left(\frac{A_{\mathrm{noz}_j}}{v_{\mathrm{exh}_j}}\left(p_{\mathrm{exh}_j} - p_{\mathrm{atm}}\right) + \dot{m}_{\mathrm{noz}_j}\right) = I_{\mathrm{sp}_j}\,g_0\,\dot{m}_{\mathrm{noz}_j}\frac{\boldsymbol{v}_{\mathrm{exh}_j}}{v_{\mathrm{exh}_j}} \tag{28}$$

For further simplicity, the cross product is substituted with the associated skew symmetric matrix, and the translational equation is written in a more compact form:

$$\begin{aligned} m_{\mathrm{sc}}\ddot{\boldsymbol{r}}_{B/N} - m_{\mathrm{sc}}\left[\tilde{\boldsymbol{c}}\right]\dot{\boldsymbol{\omega}}_{\mathcal{B}/\mathcal{N}} = {} & \boldsymbol{F}_{\mathrm{thr}} - 2\dot{m}_{\mathrm{fuel}}\left(\boldsymbol{c}' + \left[\tilde{\boldsymbol{\omega}}_{\mathcal{B}/\mathcal{N}}\right]\times\boldsymbol{c}\right) - m_{\mathrm{sc}}\boldsymbol{c}'' \\ & -2m_{\mathrm{sc}}\left[\tilde{\boldsymbol{\omega}}_{\mathcal{B}/\mathcal{N}}\right]\boldsymbol{c}' - \ddot{m}_{\mathrm{fuel}}\,\boldsymbol{c} - m_{\mathrm{sc}}\left[\tilde{\boldsymbol{\omega}}_{\mathcal{B}/\mathcal{N}}\right]\left[\tilde{\boldsymbol{\omega}}_{\mathcal{B}/\mathcal{N}}\right]\boldsymbol{c} \\ & +2\sum_{j=1}^{N}\dot{m}_{\mathrm{noz}_j}\left[\tilde{\boldsymbol{\omega}}_{\mathcal{B}/\mathcal{N}}\right]\boldsymbol{r}_{Nc_j/B} + \sum_{j=1}^{N}\ddot{m}_{\mathrm{noz}_j}\boldsymbol{r}_{Fc_j/B} \\ & +\boldsymbol{F}_{\mathrm{ext,\,vol}} + \boldsymbol{F}_{\mathrm{ext,\,surf}} \end{aligned} \tag{29}$$

This EOM is the translational equation for an open system subjected to external forces $\boldsymbol{F}_{\mathrm{ext,\,vol}}$ and $\boldsymbol{F}_{\mathrm{ext,\,surf}}$ and thrust $\boldsymbol{F}_{\mathrm{thr}} = \sum_{j=1}^{N}\boldsymbol{F}_{\mathrm{thr}_j}$ due to mass depletion of the spacecraft, represented in Fig. 1. From this equation, it can be deduced that the variation of the mass inside the spacecraft directly impacts the position of the satellite with respect to the origin as the body fixed point B changes its state of motion according to the variation of the tanks' linear inertia. In the next section, the rotational EOM for the spacecraft is developed.

Rotational Equation of Motion

The goal of this section is to develop the EOM associated with attitude dynamics of a spacecraft with depleting mass due to thrusters pulling mass from fuel tanks. Beginning from the Newton's equation:

$$\ddot{\boldsymbol{r}}_{M/N}\,\mathrm{d}m = \mathrm{d}\boldsymbol{F} \quad \Rightarrow \quad \boldsymbol{r}_{M/N} \times \ddot{\boldsymbol{r}}_{M/N}\,\mathrm{d}m = \boldsymbol{r}_{M/N} \times \mathrm{d}\boldsymbol{F} \tag{30}$$

and performing an integration over the system:

$$\int_{\text{Body}} \boldsymbol{r}_{M/N} \times \ddot{\boldsymbol{r}}_{M/N}\, \mathrm{d}m = \int_{\text{Body}} \boldsymbol{r}_{M/N} \times \mathrm{d}\boldsymbol{F} \tag{31}$$

The term on the left-hand side of the previous equation is manipulated in order to define the momentum about point B. This manipulation can be seen in the following equation:

$$\begin{aligned}\int_{\text{Body}} \rho\, \boldsymbol{r}_{M/N} \times \ddot{\boldsymbol{r}}_{M/N}\, \mathrm{d}\mathcal{V} = &\int_{\text{Body}} \rho\, \boldsymbol{r}_{M/B} \times \ddot{\boldsymbol{r}}_{M/B}\, \mathrm{d}\mathcal{V} + \int_{\text{Body}} \rho\, \boldsymbol{r}_{B/N} \times \ddot{\boldsymbol{r}}_{M/N}\, \mathrm{d}\mathcal{V} \\ &+ \int_{\text{Body}} \rho\, \boldsymbol{r}_{M/B} \times \ddot{\boldsymbol{r}}_{B/N}\, \mathrm{d}\mathcal{V} = \int_{\text{Body}} \boldsymbol{r}_{M/N} \times \mathrm{d}\boldsymbol{F}\end{aligned} \tag{32}$$

Knowing that $\ddot{\boldsymbol{r}}_{M/N}\, \mathrm{d}m = \mathrm{d}\boldsymbol{F}$, the torque caused by the forces acting on the body is easily defined:

$$\int_{\text{Body}} \boldsymbol{r}_{M/N} \times \mathrm{d}\boldsymbol{F} - \int_{\text{Body}} \rho\, \boldsymbol{r}_{B/N} \times \ddot{\boldsymbol{r}}_{M/N}\, \mathrm{d}\mathcal{V} = \int_{\text{Body}} \left(\boldsymbol{r}_{M/N} - \boldsymbol{r}_{B/N}\right) \times \mathrm{d}\boldsymbol{F} = \boldsymbol{L}_B \tag{33}$$

where $\boldsymbol{L}_B$ is the external torque on the spacecraft about point B.

As the mass of the system is constant, the derivative of the angular momentum about point B is inferred from Eq. 32 due to a property of the cross product and the previously explained Reynold's transport theorem:

$$\begin{aligned}\int_{\text{Body}} \rho\, \boldsymbol{r}_{M/B} \times \ddot{\boldsymbol{r}}_{M/B}\, \mathrm{d}\mathcal{V} = &\frac{\mathcal{N}\mathrm{d}}{\mathrm{d}t} \int_{\mathcal{V}_{\text{sc}}} \rho\, \boldsymbol{r}_{M/B} \times \dot{\boldsymbol{r}}_{M/B}\, \mathrm{d}\mathcal{V} \\ &+ \int_{\mathcal{A}_{\text{sc}}} \rho\, \boldsymbol{r}'_{M/B} \cdot \hat{\boldsymbol{n}} \left(\boldsymbol{r}_{M/B} \times \dot{\boldsymbol{r}}_{M/B}\right) \mathrm{d}A\end{aligned} \tag{34}$$

Moreover, similar to the translational equation, if all the mass of the system is assumed to be contained inside the control volume at the initial time, the following relationship results:

$$\begin{aligned}\int_{\text{Body}} \rho\, \boldsymbol{r}_{M/B} \times \ddot{\boldsymbol{r}}_{B/N}\, \mathrm{d}\mathcal{V} - \boldsymbol{L}_B = &\int_{\mathcal{V}_{\text{sc}}} \rho\, \boldsymbol{r}_{M/B} \times \ddot{\boldsymbol{r}}_{B/N}\, \mathrm{d}\mathcal{V} - \int_{\mathcal{V}_{\text{sc}}} \boldsymbol{r}_{M/B} \times \mathrm{d}\boldsymbol{F}_{\text{vol}} \\ &- \int_{\mathcal{A}_{\text{sc}}} \boldsymbol{r}_{M/B} \times \mathrm{d}\boldsymbol{F}_{\text{surf}} = m_{\text{sc}} \boldsymbol{c} \times \ddot{\boldsymbol{r}}_{B/N} \\ &- \boldsymbol{L}_{B,\,\text{vol}} - \boldsymbol{L}_{B,\,\text{surf}}\end{aligned} \tag{35}$$

where $\boldsymbol{L}_{B,\,\text{vol}}$ and $\boldsymbol{L}_{B,\,\text{surf}}$ are the torques caused by the volume and surface forces about point B. The general rotational equation for a control volume in a rotating reference frame is reorganized:

$$\dot{\boldsymbol{H}}_{\text{sc},\,B} + \int_{\mathcal{A}_{\text{sc}}} \rho\, \boldsymbol{r}'_{M/B} \cdot \hat{\boldsymbol{n}} \left(\boldsymbol{r}_{M/B} \times \dot{\boldsymbol{r}}_{M/B}\right) \mathrm{d}A + m_{\text{sc}} \boldsymbol{c} \times \ddot{\boldsymbol{r}}_{B/N} = \boldsymbol{L}_{B,\,\text{vol}} + \boldsymbol{L}_{B,\,\text{surf}} \tag{36}$$

To perform the inertial derivative of $\boldsymbol{H}_{\text{sc},\,B}$, first the definition of $\boldsymbol{H}_{\text{sc},\,B}$ is defined:

$$\boldsymbol{H}_{\text{sc},\,B} = \left[I_{\text{hub},\,B_c}\right]\boldsymbol{\omega}_{\mathcal{B}/\mathcal{N}} + \boldsymbol{r}_{Bc/B} \times m_{\text{hub}}\,\dot{\boldsymbol{r}}_{Bc/B} + \sum_{i=1}^{M}\Big(\left[I_{\text{fuel}_i,\,Fc_i}\right]\boldsymbol{\omega}_{\mathcal{B}/\mathcal{N}} + \boldsymbol{r}_{Fc_i/B} \times m_{\text{fuel}_i}\,\dot{\boldsymbol{r}}_{Fc_i/B}\Big) \tag{37}$$

where $\left[I_{\text{hub},\,B_c}\right]$ is the hub's inertia about its center of mass, B_c, and $\left[I_{\text{fuel}_i,\,Fc_i}\right]$ is the i^{th} tank's inertia about its center of mass, Fc_i. Furthermore, an analytical expression of mass depletion in the rotational motion is deduced:

$$\begin{aligned}\dot{\boldsymbol{H}}_{\text{sc},\,B} = {} & \left[I_{\text{hub},\,Bc}\right]\dot{\boldsymbol{\omega}}_{\mathcal{B}/\mathcal{N}} + \boldsymbol{\omega}_{\mathcal{B}/\mathcal{N}} \times \left(\left[I_{\text{hub},\,Bc}\right]\boldsymbol{\omega}_{\mathcal{B}/\mathcal{N}}\right) + \boldsymbol{r}_{Bc/B} \times m_{\text{hub}}\,\ddot{\boldsymbol{r}}_{Bc/B} \\ & + \sum_{i=1}^{M}\Big(\left[I_{\text{fuel}_i,\,Fc_i}\right]\dot{\boldsymbol{\omega}}_{\mathcal{B}/\mathcal{N}} + \boldsymbol{\omega}_{\mathcal{B}/\mathcal{N}} \times \left(\left[I_{\text{fuel}_i,\,Fc_i}\right]\boldsymbol{\omega}_{\mathcal{B}/\mathcal{N}}\right) \\ & + \boldsymbol{r}_{Fc_i/B} \times m_{\text{fuel}_i}\,\ddot{\boldsymbol{r}}_{Fc_i/B} + \boldsymbol{r}_{Fc_i/B} \times \dot{m}_{\text{fuel}_i}\,\dot{\boldsymbol{r}}_{Fc_i/B} + \left[I_{\text{fuel}_i,\,Fc_i}\right]'\boldsymbol{\omega}_{\mathcal{B}/\mathcal{N}}\Big)\end{aligned} \tag{38}$$

It should be noted here that any relative motion of particles inside the fuel tanks of the spacecraft has been neglected and, as a consequence, the effects both of the Coriolis' acceleration and of the whirling motion of the fuel on the spacecraft dynamics have not been considered. A more detailed explanation of the impact of these effects can be found in Reference [8].

Additionally, the inertial time derivatives of the vectors $\boldsymbol{r}_{Bc/B}$ and $\boldsymbol{r}_{Fc_i/B}$ are computed using the transport theorem between the two reference frames given in Eqs. 7 and 8 and considering that the point B_c is fixed in the $\mathcal{B}$ frame, Eq. 38 is rewritten:

$$\begin{aligned}\dot{\boldsymbol{H}}_{\text{sc},\,B} = {} & \left[I_{\text{hub},\,Bc}\right]\dot{\boldsymbol{\omega}}_{\mathcal{B}/\mathcal{N}} + \boldsymbol{\omega}_{\mathcal{B}/\mathcal{N}} \times \left(\left[I_{\text{hub},\,Bc}\right]\boldsymbol{\omega}_{\mathcal{B}/\mathcal{N}}\right) \\ & + \boldsymbol{r}_{Bc/B} \times m_{\text{hub}}\left(\dot{\boldsymbol{\omega}}_{\mathcal{B}/\mathcal{N}} \times \boldsymbol{r}_{Bc/B} + \boldsymbol{\omega}_{\mathcal{B}/\mathcal{N}} \times \left(\boldsymbol{\omega}_{\mathcal{B}/\mathcal{N}} \times \boldsymbol{r}_{Bc/B}\right)\right) \\ & + \sum_{i=1}^{M}\Big(\left[I_{\text{fuel}_i,\,Fc_i}\right]\dot{\boldsymbol{\omega}}_{\mathcal{B}/\mathcal{N}} + \boldsymbol{\omega}_{\mathcal{B}/\mathcal{N}} \times \left(\left[I_{\text{fuel}_i,\,Fc_i}\right]\boldsymbol{\omega}_{\mathcal{B}/\mathcal{N}}\right) \\ & + \boldsymbol{r}_{Fc_i/B} \times m_{\text{fuel}_i}\left(\boldsymbol{r}''_{Fc_i/B} + 2\,\boldsymbol{\omega}_{\mathcal{B}/\mathcal{N}} \times \boldsymbol{r}'_{Fc_i/B} + \dot{\boldsymbol{\omega}}_{\mathcal{B}/\mathcal{N}} \times \boldsymbol{r}_{Fc_i/B}\right. \\ & \left. + \boldsymbol{\omega}_{\mathcal{B}/\mathcal{N}} \times \left(\boldsymbol{\omega}_{\mathcal{B}/\mathcal{N}} \times \boldsymbol{r}_{Fc_i/B}\right)\right) + \boldsymbol{r}_{Fc_i/B} \\ & \times \dot{m}_{\text{fuel}_i}\left(\boldsymbol{r}'_{Fc_i/B} + \boldsymbol{\omega}_{\mathcal{B}/\mathcal{N}} \times \boldsymbol{r}_{Fc_i/B}\right) + \left[I_{\text{fuel},_i,\,Fc_i}\right]'\boldsymbol{\omega}_{\mathcal{B}/\mathcal{N}}\Big)\end{aligned} \tag{39}$$

In order to simplify Eq. 39 the following inertia matrices are defined using the skew symmetric matrix to replace the cross product:

$$\left[I_{\text{hub},\,B}\right] = \left[I_{\text{hub},\,Bc}\right] + m_{\text{hub}}\left[\tilde{\boldsymbol{r}}_{Bc/B}\right]\left[\tilde{\boldsymbol{r}}_{Bc/B}\right]^T \tag{40}$$

$$\left[I_{\text{fuel}_i,\,B}\right] = \left[I_{\text{fuel}_i,\,Fc_i}\right] + m_{\text{fuel}_i}\left[\tilde{\boldsymbol{r}}_{Fc_i/B}\right]\left[\tilde{\boldsymbol{r}}_{Fc_i/B}\right]^T \tag{41}$$

$$\left[I_{\text{sc},\,B}\right] = \left[I_{\text{hub},\,B}\right] + \sum_{i=1}^{M}\left[I_{\text{fuel}_i,\,B}\right] \tag{42}$$

Moreover, using the Jacobi identity for the cross product $\mathbf{a}\times(\mathbf{b}\times\mathbf{c})+\mathbf{b}\times(\mathbf{c}\times\mathbf{a})+\mathbf{c}\times(\mathbf{a}\times\mathbf{b})=\mathbf{0}$, the body relative time derivative of the fuel inertia in the $\mathcal{B}$ reference frame is introduced:

$$\begin{aligned}\left[I_{\text{fuel}_i,\,B}\right]' &= \left[I_{\text{fuel}_i,\,Fc_i}\right]+\dot{m}_{\text{fuel}_i}\left[\tilde{\boldsymbol{r}}_{Fc_i/B}\right]\left[\tilde{\boldsymbol{r}}_{Fc_i/B}\right]^T\\ &\quad+m_{\text{fuel}_i}\left(\left[\tilde{\boldsymbol{r}}_{Fc_i/B}\right]\left[\tilde{\boldsymbol{r}}'_{Fc_i/B}\right]^T+\left[\tilde{\boldsymbol{r}}'_{Fc_i/B}\right]\left[\tilde{\boldsymbol{r}}_{Fc_i/B}\right]^T\right)\end{aligned}\tag{43}$$

By substituting Eqs. 40–43, Eq. 39 is simplified to:

$$\begin{aligned}\dot{\boldsymbol{H}}_{\text{sc},\,B} &= \left[I_{\text{sc},\,B}\right]\dot{\boldsymbol{\omega}}_{\mathcal{B}/\mathcal{N}}+\left[\tilde{\boldsymbol{\omega}}_{\mathcal{B}/\mathcal{N}}\right]\left[I_{\text{sc},\,B}\right]\boldsymbol{\omega}_{\mathcal{B}/\mathcal{N}}\\ &\quad+\sum_{i=1}^{M}\Big(m_{\text{fuel}_i}\left[\tilde{\boldsymbol{r}}_{Fc_i/B}\right]\boldsymbol{r}''_{Fc_i/B}+\dot{m}_{\text{fuel}_i}\left[\tilde{\boldsymbol{r}}_{Fc_i/B}\right]\boldsymbol{r}'_{Fc_i/B}\\ &\quad+\left[I_{\text{fuel}_i,\,B}\right]'\boldsymbol{\omega}_{\mathcal{B}/\mathcal{N}}+\left[\tilde{\boldsymbol{\omega}}_{\mathcal{B}/\mathcal{N}}\right]\left[\tilde{\boldsymbol{r}}_{Fc_i/B}\right]\boldsymbol{r}'_{Fc_i/B}\Big)\end{aligned}\tag{44}$$

Considering that at the nozzles's exit $\dot{\boldsymbol{r}}_{M/B}=\boldsymbol{v}_{exh_j}+\boldsymbol{\omega}_{\mathcal{B}/\mathcal{N}}\times\boldsymbol{r}_{M/B}$ and $\mathrm{d}\dot{m}=-\rho\,\boldsymbol{r}'_{M/B}\cdot\hat{\boldsymbol{n}}\,\mathrm{d}A$ because the control volume is fixed, the surface integral is expressed in terms of the nozzles' surface:

$$\begin{aligned}\int_{A_{\text{exh}}}\rho\,\boldsymbol{r}'_{M/B}\cdot\boldsymbol{n}\left(\boldsymbol{r}_{M/B}\times\dot{\boldsymbol{r}}_{M/B}\right)\mathrm{d}A &= -\sum_{j=1}^{N}\int_{\dot{m}_{\text{noz}_j}}\boldsymbol{r}_{M/B}\times\boldsymbol{v}_{\text{exh}_j}\,\mathrm{d}\dot{m}\\ &\quad+\sum_{j=1}^{N}\int_{\dot{m}_{\text{noz}_j}}\boldsymbol{r}_{M/B}\\ &\quad\times\left(\boldsymbol{r}_{M/B}\times\boldsymbol{\omega}_{\mathcal{B}/\mathcal{N}}\right)\mathrm{d}\dot{m}\end{aligned}\tag{45}$$

Equation 36 is updated with Eqs. 44 and 45:

$$\begin{aligned}&\left[I_{\text{sc},\,B}\right]\dot{\boldsymbol{\omega}}_{\mathcal{B}/\mathcal{N}}+\left[\tilde{\boldsymbol{\omega}}_{\mathcal{B}/\mathcal{N}}\right]\left[I_{\text{sc},\,B}\right]\boldsymbol{\omega}_{\mathcal{B}/\mathcal{N}}+\sum_{i=1}^{M}\Big(m_{\text{fuel}_i}\left[\tilde{\boldsymbol{r}}_{Fc_i/B}\right]\boldsymbol{r}''_{Fc_i/B}\\ &\quad+\left[I_{\text{fuel}_i,\,B}\right]'\boldsymbol{\omega}_{\mathcal{B}/\mathcal{N}}+\dot{m}_{\text{fuel}_i}\left[\tilde{\boldsymbol{r}}_{Fc_i/B}\right]\boldsymbol{r}'_{Fc_i/B}\\ &\quad+m_{\text{fuel}_i}\left[\tilde{\boldsymbol{\omega}}_{\mathcal{B}/\mathcal{N}}\right]\left[\tilde{\boldsymbol{r}}_{Fc_i/B}\right]\boldsymbol{r}'_{Fc_i/B}\Big)+\sum_{j=1}^{N}\int_{\dot{m}_{\text{noz}_j}}\left[\tilde{\boldsymbol{r}}_{M/B}\right]^T\boldsymbol{v}_{\text{exh}_j}\,\mathrm{d}\dot{m}\\ &\quad+\sum_{j=1}^{N}\int_{\dot{m}_{\text{noz}_j}}\left[\tilde{\boldsymbol{r}}_{M/B}\right]\left[\tilde{\boldsymbol{r}}_{M/B}\right]\boldsymbol{\omega}_{\mathcal{B}/\mathcal{N}}\,\mathrm{d}\dot{m}\\ &\quad+\left[\tilde{\boldsymbol{c}}\right]m_{\text{sc}}\ddot{\boldsymbol{r}}_{B/N}=\boldsymbol{L}_{B,\,\text{vol}}+\boldsymbol{L}_{B,\,\text{surf}}\end{aligned}\tag{46}$$

The torque of each thruster nozzle is computed by the exhausting flow pressure distribution and by the lever arm distance from point B and the application point of the force:

$$\boldsymbol{L}_{B_{\text{thr}_j}}=\boldsymbol{L}_{B_{\text{sc, noz}_j}}+\int_{\dot{m}_{\text{noz}_j}}\boldsymbol{r}_{M/B}\times\boldsymbol{v}_{\text{noz}_j}\,\mathrm{d}\dot{m}\tag{47}$$

Furthermore, a term taking into account the angular momentum variation caused by mass depletion is defined:

$$[K] = \sum_{i=1}^{M} \left[I_{\text{fuel}_i,\,B}\right]' + \sum_{j=1}^{N} \int_{\dot{m}_{\text{noz}_j}} \left[\tilde{\boldsymbol{r}}_{M/B}\right]\left[\tilde{\boldsymbol{r}}_{M/B}\right] \mathrm{d}\dot{m} \tag{48}$$

Equation 48 is important because this is what drives the dynamical effect of the fully coupled mass depletion model. The difference between the changing mass properties in the full tank to the exhausted fuel at the nozzle locations is what produces a torque on the spacecraft. The quantities $\left[I_{\text{fuel}_i,\,B}\right]$ and $\left[I_{\text{fuel}_i,\,B}\right]'$ depend on the chosen tank model and some examples can be seen in the Appendix. Interchanging tank models does not change the overall EOMs and other type of models can be developed depending on the application. The second integral in Eq. 48 is computed evaluating the momentum exchanged due to the fuel exiting the nozzle area, coincident with the interface surface between the spacecraft and the exhausted fuel and supposed circular:

$$\begin{aligned}\int_{\dot{m}_{\text{noz}_j}} \left[\tilde{\boldsymbol{r}}_{M/B}\right]\left[\tilde{\boldsymbol{r}}_{M/B}\right] \mathrm{d}\dot{m} \;=\; & \int_{\dot{m}_{\text{noz}_j}} \left(\left[\tilde{\boldsymbol{r}}_{Nc_j/B}\right] + \left[\tilde{\boldsymbol{r}}_{M/Nc_j}\right]\right)\left(\left[\tilde{\boldsymbol{r}}_{Nc_j/B}\right]\right. \\ & \left. + \left[\tilde{\boldsymbol{r}}_{M/Nc_j}\right]\right) \mathrm{d}\dot{m} = -\dot{m}_{\text{noz}_j}\left(\left[\tilde{\boldsymbol{r}}_{Nc_j/B}\right]\left[\tilde{\boldsymbol{r}}_{Nc_j/B}\right]^T\right. \\ & \left. + \frac{A_{\text{noz}_j}}{4\,\pi}\left[BM_j\right]\begin{bmatrix} 2 & 0 & 0 \\ 0 & 1 & 0 \\ 0 & 0 & 1 \end{bmatrix}\left[BM_j\right]^T\right)\end{aligned} \tag{49}$$

where A_{noz_j} is the exiting area of the j^{th} nozzle and $\left[BM_j\right]$ is the direction cosine matrix (DCM) between the j^{th} nozzle frame $\mathcal{M}_j$ and the $\mathcal{B}$ frame, where $\mathcal{M}_j$ is defined to have its origin at the Nc_j point and its first axis in the exhausting velocity direction $\boldsymbol{v}_{\text{exh}_j}$. An important aspect of Eq. 49 is that the assumption of a circular surface has been chosen to obtain an analytical closed form of the EOM. However, the previously derived term can be easily adapted to a more complex surface geometry by changing the matrix between the two DCMs at the end of Eq. 49 with the inertia matrix associated with the mass surface of each nozzle.

Finally the rotational EOM is written as:

$$\begin{aligned}\left[I_{\text{sc},\,B}\right]\dot{\boldsymbol{\omega}}_{\mathcal{B}/\mathcal{N}} + m_{\text{sc}}\left[\tilde{\boldsymbol{c}}\right]\ddot{\boldsymbol{r}}_{B/N} \;=\; & -\left[\tilde{\boldsymbol{\omega}}_{\mathcal{B}/\mathcal{N}}\right]\left[I_{\text{sc},\,B}\right]\boldsymbol{\omega}_{\mathcal{B}/\mathcal{N}} - [K]\,\boldsymbol{\omega}_{\mathcal{B}/\mathcal{N}} \\ & + \sum_{i=1}^{M}\left(m_{\text{fuel}_i}\left[\tilde{\boldsymbol{r}}_{Fc_i/B}\right]^T\boldsymbol{r}''_{Fc_i/B}\right. \\ & + m_{\text{fuel}_i}\left[\tilde{\boldsymbol{\omega}}_{\mathcal{B}/\mathcal{N}}\right]^T\left[\tilde{\boldsymbol{r}}_{Fc_i/B}\right]\boldsymbol{r}'_{Fc_i/B} \\ & \left. + \dot{m}_{\text{fuel}_i}\left[\tilde{\boldsymbol{r}}_{Fc_i/B}\right]^T\boldsymbol{r}'_{Fc_i/B}\right) + \boldsymbol{L}_{B,\,\text{vol}} \\ & + \boldsymbol{L}_{B,\,\text{surf}} + \sum_{j=1}^{N}\boldsymbol{L}_{B_{\text{thr}_j}}\end{aligned} \tag{50}$$

This concludes the derivation of the EOMs needed to describe the translational and rotational motion of a spacecraft with depleting mass due to thrusters. The following section describes a method used to implement the mass flow relationship between thrusters and fuel tanks.

Fuel Supply Architecture and Implementation

This section connects how the fuel expelled at each thruster causes a fuel talk or fuel reserve to change its mass properties. As mentioned earlier, the fuel flow within the piping is ignored in this analysis as being higher order. A set of thruster may draw fuel from the same tank, or a set of tanks. During flight the fuel-draw may be switched to an auxiliary tank. The following development illustrates how the presented formulation can be flexibly connected with a range of fuel storage configurations. This makes it convenient to implement in modular astrodynamics simulation such as the Basilisk framework. Alcorn et al. [18, 19]

From a software implementation prospective, the tank mass flow rates and their associated derivatives must be computed to evaluate the different terms in the EOMs. This approach assumes that the j^{th} nozzle mass flow is a known quantity and is computed using Eq. 28 and then the tanks' mass variation $\dot{m}_{\text{fuel}_i}$ is computed. If a thruster firing is numerically simulated the computational thruster model contains information about its fuel efficiency through the I_{sp} parameter. By knowing what force the thruster model is producing, the I_{sp} value allows Eq. 28 to be solved for the associated thruster fuel mass flow. If the thruster control solution is requiring a variable thrust implementation, or the computational thruster model contains on- and off-ramping to the steady-state thrust force, then the mass flow acceleration values would be obtained from this thruster model.

The i^{th} tank's mass variation is expressed as a linear combination of the fuel ejected by the nozzle where the coefficient, A_{ij}, linking the i^{th} tank with the j^{th} nozzle is the ratio of the mass released by the tank flowing to that nozzle to the total mass released by that tank.

$$\dot{m}_{\text{fuel}_i} = \sum_{j=1}^{N} A_{ij}\, \dot{m}_{\text{noz}_j} \tag{51}$$

A matrix notation can also be used:

$$\dot{\boldsymbol{m}}_{\text{fuel}} = [A]\, \dot{\boldsymbol{m}}_{\text{noz}} \tag{52}$$

where $[A]$ is a matrix linking the tanks' and nozzles' mass flow rates. A fundamental property of the matrix $[A]$ is established from the definition of $\dot{m}_{\text{fuel}}$:

$$\sum_{i=1}^{M} \dot{m}_{\text{fuel}_i} = \sum_{i=1}^{M}\sum_{j=1}^{N} A_{ij}\dot{m}_{\text{noz}_j} = \sum_{j=1}^{N} \dot{m}_{\text{noz}_j} \quad \Rightarrow \quad \sum_{i=0}^{M} A_{ij} = 1 \quad \forall j \in (1, N) \tag{53}$$

The previous relation is a direct consequence of the mass flow conservation between the tanks and the nozzles and is used in the flight software implementation to verify

inputs consistency. From the previous relation, the first derivative of mass flows is computed:

$$\ddot{\boldsymbol{m}}_{\text{fuel}} = [A]\ \ddot{\boldsymbol{m}}_{\text{noz}} + [\dot{A}]\dot{\boldsymbol{m}}_{\text{noz}} \tag{54}$$

This architecture takes into account connections among tanks and thrusters in a straightforward formulation and allows the implementation of both changes in propellant chemical composition and of switching among tanks.

In Fig. 3 an example of a possible distribution system is shown. Taking into account this schematic representation and the fact that each component of the matrix A_{ij} represent the ratio of fuel ejected by the nozzle j given from the tank i, an example is developed. The resulting equations are:

$$\dot{m}_{\text{fuel}_1} = \dot{m}_{\text{noz}_1} + \dot{m}_{\text{noz}_2} \tag{55a}$$

$$\dot{m}_{\text{fuel}_2} = 0.3\,\dot{m}_{\text{noz}_4} + \dot{m}_{\text{noz}_5} \tag{55b}$$

$$\dot{m}_{\text{fuel}_3} = \dot{m}_{\text{noz}_3} + 0.7\,\dot{m}_{\text{noz}_4} \tag{55c}$$

Thus, the corresponding $[A]$ matrix for the configuration in Fig. 3 is:

$$[A] = \begin{bmatrix} 1 & 1 & 0 & 0 & 0 \\ 0 & 0 & 0 & 0.3 & 1 \\ 0 & 0 & 1 & 0.7 & 0 \end{bmatrix} \tag{56}$$

By considering the assumptions of the model, the following points should be noted:

- There is no difference between solid and liquid propellant in a tank except for how the mass distribution could vary inside the tank itself, the propellant density and the I_{sp}. From this point of view, different tank models that specify how expelled fuel mass impact the tank inertia properties can be chosen without needing to changing the underlining EOMs. Some examples of tank models are

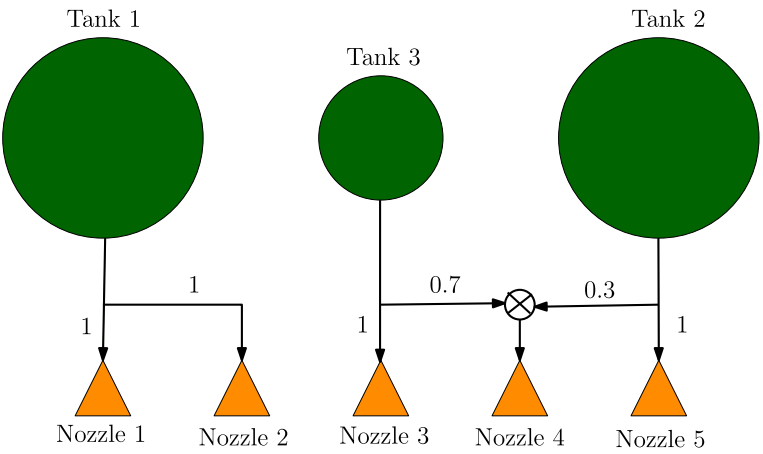

Fig. 3 An example of the distribution system among tanks and nozzles with numerical values

summarized in the Appendix, but other tank models can be developed depending on the application.

- Thrust modulation, for example throttling, does not change the EOMs because force of the j^{th} nozzle modifies through the Tsiolkovsky formula, $F_{\text{thr}_j} = g_0 I_{\text{sp}_j} \dot{m}_{\text{noz}_j}$, and the mass flow is regulated accordingly through the $[A]$ matrix.
- The model assumes that the thrust forces are known. From this information, $\dot{m}_{\text{noz}_j}$ and $\dot{m}_{\text{fuel}_i}$ are computed accordingly by knowing $[A]$, $[\dot{A}]$ and I_{sp_j} for each thruster and tank.

Results

This section provides simulations to both validate the EOMs developed and to show the impact of mass depletion on a specific scenario. In the first example, a simulation is developed to compare results to prior developed models. Following this, an example is included that involves a fuel demanding maneuver that highlights the importance of considering mass depletion for high-accuracy pointing, simulation and control law design.

Validating Simulations: Axial-symmetric Rocket

The following simulations are performed to reproduce the results outlined in Reference [5] in order to validate the dynamical model developed versus the model seen in Reference 5 which assumes that the spacecraft is axial-symmetric. The spacecraft under study is an axial-symmetric rocket represented in Fig. 4 where the geometrical features of the rocket are shown.

There are two tank models considered for this simulation: a centrifugal burn tank and a uniform cylinder tank. The models used for these tanks can be seen in Reference [5] and are reported in the Appendix for the sake of completeness. The numerical values used in the simulations are chosen accordingly with the NASA pub-

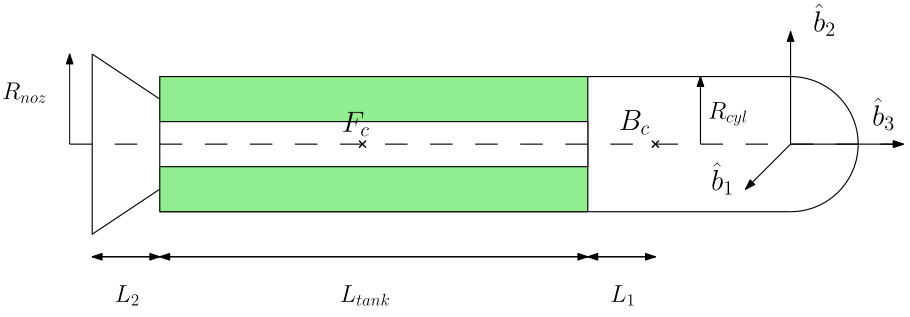

Fig. 4 Geometrical properties of the axial-symmetrical rocket

Table 1 Dimensionless parameters for the axial-symmetrical rocket simulation

δ_1	δ_2	γ_1	γ_2	α	δ	ψ
2	3	1.2	1	0.01	10	2

lication [5]. In the publication, dimensionless variables are used and their primitive definitions can be found using the following formulas:

$$\beta = \frac{R_{\text{noz}}}{R_{\text{cyl}}} \qquad \delta_1 = \frac{L_1}{R_{\text{cyl}}} \qquad \delta_2 = \frac{L_2}{R_{\text{cyl}}} \qquad \delta = \frac{L}{R_{\text{cyl}}}$$
$$\psi = \frac{m_{\text{hub}}}{m_{\text{fuel}_0}} \qquad \gamma_1 = \frac{k_{\text{hub}_{12}}}{R_{\text{cyl}}} \qquad \gamma_2 = \frac{k_{\text{hub}_3}}{R_{\text{cyl}}} \qquad \alpha = \frac{\dot{m}_{\text{fuel}}}{m_{\text{fuel}_0}}$$

where $k_{\text{hub}_{12}}$ is the hub's gyration radius of the $\hat{\boldsymbol{b}}_1$ or the $\hat{\boldsymbol{b}}_2$ about the B_c point and k_{hub_3} is the hub's gyration radius of the $\hat{\boldsymbol{b}}_3$ about the same point. The numerical dimensionless coefficients' values are reported in Table 1.

The spin rate, $\boldsymbol{\omega}_{\mathcal{B}/\mathcal{N}_z}$, is presented for the two tank's cases given in Reference [5]. This quantity is defined as follows:

$$\boldsymbol{\omega}_{\mathcal{B}/\mathcal{N}_z} = \boldsymbol{\omega}_{\mathcal{B}/\mathcal{N}} \cdot \hat{\boldsymbol{b}}_3 \tag{57}$$

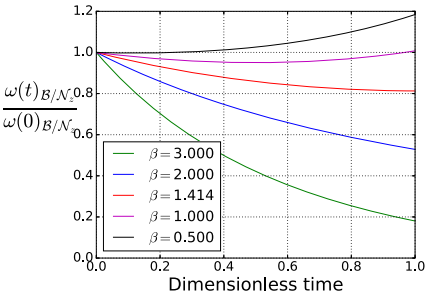

(a) Cetrifugal burn tank with developed model

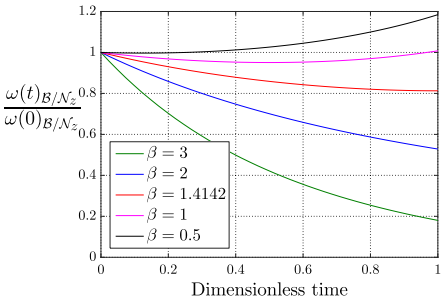

(b) Cetrifugal burn tank with Reference 5's model

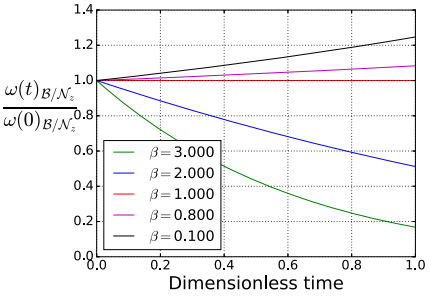

(c) Uniform cylinder tank with developed model

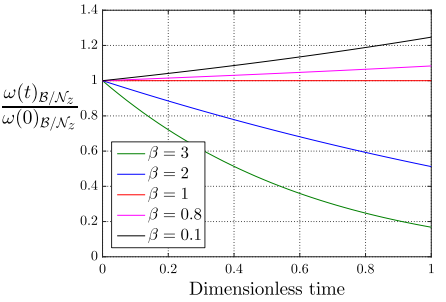

(d) Uniform burn tank with Reference 5's model

Fig. 5 Spinning rate $\boldsymbol{\omega}_{\mathcal{B}/\mathcal{N}_z}$ evolution in time comparing the developed model and Reference [5]'s model

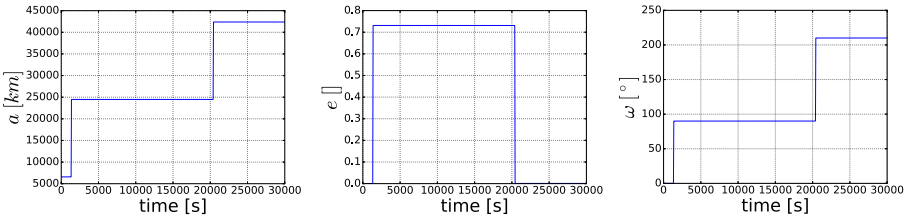

(a) Semi-major axis a (b) Eccentricity e (c) Argument of the periapsis ω

Fig. 6 Variation of main orbital parameters during the LEO-to-GEO transfer

Figure 5 shows that the behavior of the angular velocity for the entirety of the simulation match the previous work from Reference [5]. Furthermore, Fig. 5a and c present the results obtained by the direct integration of the model developed in the present paper while Fig. 5b and d display the integration of the dimensionless model introduced in Reference [5]. These results give partial validation of the model introduced in this work. It is important to point out, however, that the model presented in this paper does not constrain the analysis to axial-symmetric bodies or to a single-tank and single-thruster spacecraft. It is developed in a general way that can apply to many spacecraft configurations.

On-orbit Spacecraft Simulations: LEO-to-GEO Transfer

The goal of the following closed-loop attitude control maneuver is to illustrate how the depletable mass dynamics model can impact the control solution. For this purpose a scenario is studied where the spacecraft attitude is regulated while fuel is expelled to perform a large orbit maneuver. A geostationary transfer maneuver from LEO (Low Earth Orbit) to GEO (Geostationary Earth Orbit) using a Hohmann transfer maneuver is implemented (see Fig. 6). The orbital elements of the initial, the transfer orbit, and the final orbit are included in Table 2. To isolate the impacts of mass depletion, a two-body-problem gravity field is considered and no gravity torque perturbation is included.

In order to give a meaningful example using the EOMs developed, a control law is introduced. The control is included to reach the desired reference state despite disturbances applied on the spacecraft. A Modified Rodrigues Parameters (MRP)

Table 2 Orbital element for the Hohmann maneuver

	a [km]	e [ ]	i [°]	ω [°]	Ω [°]
Low earth orbit	6578.0	0.0	0.0	0.0	0.0
Hohmann transfer orbit	24478.0	0.73126	0.0	90.0	0.0
Geostationary earth orbit	42378.0	0.0	0.0	0.0	0.0

Table 3 Geometrical characteristics of the satellite for the Hohmann transfer

m_{hub} [kg]	$I_{\text{hub, }Bc_{11}}$ [kg m^2]	$I_{\text{hub, }Bc_{22}}$ kg m^2]	$I_{\text{hub, }Bc_{33}}$ [kg m^2]	
750.0	900.0	800.0	600.0	
I_{sp_j} [s]	m_{tank_i} [kg]	A_{noz_j} [m^2]	A_{noz_j}[m^2]	R_{tank_i} [m]
$\forall j \in [1,\ 14]$	$\forall i \in [1,\ 2]$	$\forall j \in [3,\ 14]$	$\forall j \in [1,\ 2]$	$\forall i \in [1,\ 2]$
300.0	1060.0	0.07	0.2	0.5

feedback control law is chosen and, if a reference frame $\mathcal{R}$ is defined, the control is expressed as follows:

$$\boldsymbol{u} = -K\,\boldsymbol{\sigma}_{\mathcal{B}/\mathcal{R}} - P\,\boldsymbol{\omega}_{\mathcal{B}/\mathcal{R}} \tag{58}$$

where $\boldsymbol{\sigma}_{\mathcal{B}/\mathcal{R}}$ is the MRP defining the attitude of $\mathcal{B}$ with respect to $\mathcal{R}$ and $\boldsymbol{\omega}_{\mathcal{B}/\mathcal{R}}$ is the angular velocity of $\mathcal{B}$ with respect to $\mathcal{R}$. In order to evaluate the control torque, the attitude $\boldsymbol{\sigma}_{\mathcal{B}/\mathcal{R}}$ and the angular velocity $\boldsymbol{\omega}_{\mathcal{B}/\mathcal{R}}$ must be computed. $\boldsymbol{\sigma}_{\mathcal{R}/\mathcal{N}}$ and $\boldsymbol{\omega}_{\mathcal{R}/\mathcal{N}}$ are assumed to be specified by the controller by using information about the desired reference frame, $\mathcal{R}$. Schaub and Junkins [20] Moreover, to avoid singularities of the MRP set $\boldsymbol{\sigma}_{\mathcal{B}/\mathcal{R}}$, the MRP can be switched to the shadow set representation [20].

In this scenario, the satellite has a 12-ADC nozzle cluster in a symmetric configuration to control the attitude of the spacecraft and it is equipped with two delta-velocity (DV) thrusters to perform the firing at apogee and at perigee of the elliptic orbit. Two spherical constant volume tanks, using the constant volume model seen in the Appendix, provide the fuel for the ACS and DV thrusters. The geometrical features are presented in Table 3. Furthermore, the initial conditions for the dynamic variables and the chosen simulation parameters are listed in Table 4.

Three scenarios are simulated for this example to highlight the impact of mass depletion on the dynamics of the spacecraft. An "Update-Only" simulation is the first scenario considered and is very commonly used in industry. This involves only updating the current mass properties of the spacecraft but not considering the influence of mass depletion on the system. Additionally, there is not a control law on the attitude of the spacecraft implemented in this scenario. In contrast, the second scenario is named "No-Control" and is a scenario in which the attitude and attitude rate of the satellite is not being controlled, however, this scenario does use the full dynamical model developed in this paper. Lastly, the "Active-Control" scenario uses the developed model along with the previously introduced attitude control law.

The initial conditions specified in Table 4, along with assumptions being made will constrict the satellite to only rotate about the $\hat{\boldsymbol{b}}_1$ axis. Therefore, the numerical results

Table 4 Hohmann transfer simulation parameters

$t_{\text{in}}\,[s]$	$t_{\text{fin}}\,[s]$	$\Delta t\,[s]$	$\boldsymbol{\sigma}_{\mathcal{R}/\mathcal{N}}$ [ ]	$\boldsymbol{\omega}_{\mathcal{R}/\mathcal{N}}\,[rad\,s^{-1}]$
0.0	30000.0	0.01	$[0,\ 0,\ 0\,]^T$	$[0.002,\ 0,\ 0\,]^T$
$\boldsymbol{r}_{B/N_0}\,[m]$	$\dot{\boldsymbol{r}}_{B/N_0}\,[m\,s^{-1}]$	$\boldsymbol{\sigma}_{\mathcal{B}/\mathcal{N}_0}$ [ ]	$\boldsymbol{\omega}_{\mathcal{B}/\mathcal{N}_0}\,[rad\,s^{-1}]$	
$[a_{LEO},\ 0,\ 0\,]^T$	$\left[0,\ \sqrt{\frac{\mu}{a_{LEO}}},\ 0\right]^T$	$[0,\ 0,\ 0\,]^T$	$[0.002,\ 0,\ 0\,]^T$	

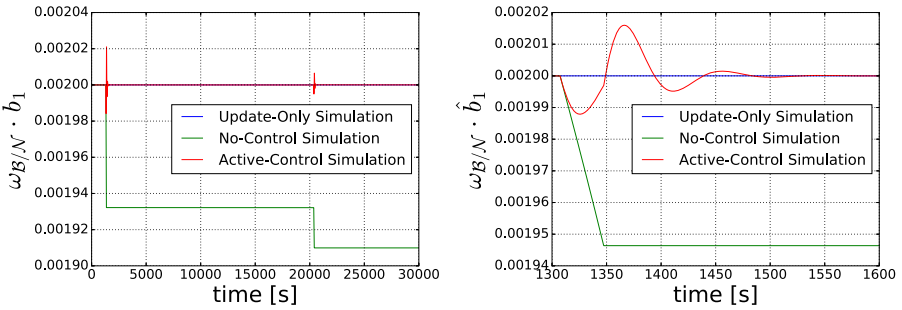

(a) General behavior for the coplete simuation. (b) Details for the first firing period.

Fig. 7 Projection of $\boldsymbol{\omega}_{\mathcal{B}/\mathcal{N}}$ on the $\hat{\boldsymbol{b}}_3$ axis

between the "Update-Only" and the "No-Control" scenarios will directly show the impact of mass depletion on the dynamics of the satellite. The numerical results of the simulation are presented in Figs. 7 and 8. Figures 8a and b are included to show the mass variation of the system.

In Figs. 7a and b the angular velocity about the $\hat{\boldsymbol{b}}_1$ axis is shown. In Fig. 7a, the complete 75 hr simulation is presented to compare the previously listed simulations. By comparing the "Update-Only" scenario with the "No-Control" scenario, there is a noticeable difference in the angular velocity of the system which is caused by the dynamical effects introduced by the mass depletion. The fact that the angular velocity variation in the "No-Control" case is negative along with the magnitude of the angular velocity variation are due to the DV thrusters' configuration, both in term of position and geometry, and the tanks' location and dimension as seen in Eq. 48. Obviously changing the properties of either one of the two features will lead to a different solution in terms of amplitude and sign. The results show that the "Update-Only" scenario does not show any change to the angular velocity due to mass depletion, while the "No-Control" case does. This difference can lead to a

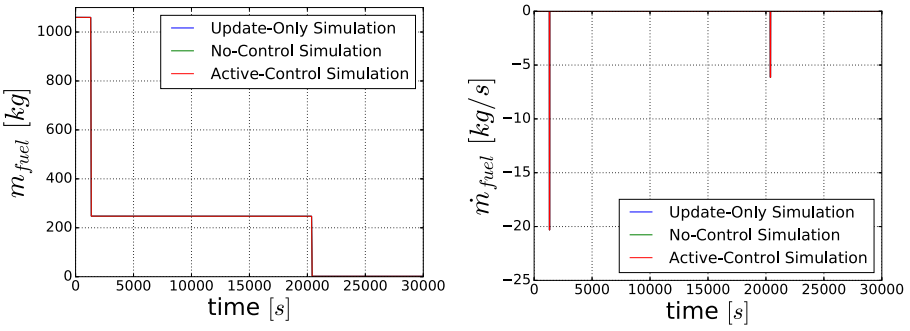

(a) m_{fuel} (b) $\dot{m}_{\text{fuel}}$

Fig. 8 Mass variation during the Hohmann maneuver simulation

dramatic differences in results and gives importance to the model developed in this paper. In this particular case, the error introduced by mass depletion is about 4 %.

In Fig. 7a, a portion of the first DV burn is displayed to get a better view of the transient. This result is important because it highlights the difference between the "Update-Only" and the "Active-Control" scenarios. As discussed previously, this shows that the "Update-Only" approach indicates no change in the angular velocity. However, with the dynamics developed in this paper, to keep the spacecraft with the desired angular velocity, the "Active-Control" shows that control is required and the the transient due to the ACS thrusters controlling the spacecraft can be seen in Fig. 7b.

Conclusions

A review of the previous work on the dynamics of spacecraft with mass depletion due to thrusters shows that the assumptions being made limit the applicability of the models to many spacecraft. This work develops the translational and rotational EOMs while keeping the formulation as general as possible to avoid this issue. This results in arriving at a complete solution that gets rid of the need to rederive the EOMs for specific spacecraft. A novel and compact form of the EOMs is introduced in the case of a realistic multi-tank and multi-thruster configuration that provides rapid and efficient formulation to perform simulations. Additionally, the general derivation allows the model to be expanded quite easily to include effects like panels' deployment or flexible structures, without loss of generality.

The model is validated by comparing a simulation to prior models on mass depletion. This gives confidence in the formulation developed. Again, these prior models have assumptions that limit the scope of applicability and this comparison is purely for validation purposes. The importance of considering mass depletion is proven by comparing the full model developed in this paper with a solution where the mass properties of the spacecraft are just updated each time step. This gives an error of 4 % on the spacecraft angular velocity with the chosen geometrical features. Depending on the scenario, this error could be much worse and highlights the main desire to consider mass depletion using this model. Ignoring these effects of mass depletion could lead to hastened de-saturation maneuvers or cause inaccurate pointing and unpredicted errors in orientation and position of the spacecraft.

Some limiting assumptions are introduced to this model that does not allow the EOMs to consider the effect of whirling motions or relative fuel motion in the distribution of the system. Future works could consider the influence of whirling motion using a simple formulation or introduction of reaction wheels to simulate complex de-saturation maneuvers.

Acknowledgments This work was supported by the Italian Space Agency (ASI) in collaboration with the Cultural Association of Italians at Fermilab (CAIF).

Appendix

This appendix summarizes how a series of tank models [5] relate the fuel mass flow rate (expelled from the thruster) to the tank inertia and inertia rate properties. All the models have a fixed center of mass and this results in $\boldsymbol{r}'_{Tc/B} = 0$ and $\boldsymbol{r}''_{Tc/B} = 0$.

Tanks which are more complex than the ones presented in the following paragraphs can be implemented by the user thanks to the modularity and generality of the exposed model.

Uniform burn cylinder

This model considers a cylindrical tank whose geometry remains constant while fuel density changes. From these considerations and by looking at Fig. 9a, the inertia tensor and its derivative are evaluated:

$$I_{11} = I_{22} = m_{\text{fuel}} \left[\frac{R^2}{4} + \frac{h^2}{3} \right] \qquad I_{33} = m_{\text{fuel}} \frac{R^2}{2} \tag{59}$$

$$I'_{11} = I'_{22} = \dot{m}_{\text{fuel}} \left[\frac{R^2}{4} + \frac{h^2}{3} \right] \qquad I'_{33} = \dot{m}_{\text{fuel}} \frac{R^2}{2} \tag{60}$$

where R is the cylinder radius and h its half-height.

Centrifugal burn cylinder

This model considers a cylinder whose propellant burns radially from the center till the edge. The geometry properties and their nomenclature is presented in Fig. 9b. By denoting r the distance of the fuel surface from the axis of the cylinder:

$$r = \sqrt{R^2 - \frac{m_{\text{fuel}}}{2\,\pi\,\rho\,h}} \tag{61}$$

where R is the cylinder radius, h its half-height and ρ the fuel density.

The time derivative of r is gathered from volume-mass relationship:

$$\dot{m}_{\text{fuel}} = -4\pi\rho\,h\,r\,\dot{r} \tag{62}$$

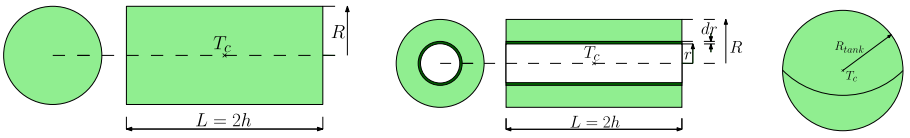

(a) Uniform burn cylinder (b) Centrifugal burn cylinder (c) Constant volume tank

Fig. 9 Tanks' geometrical properties

As a consequence:

$$I_{11} = I_{22} = m_{\text{fuel}} \left[\frac{R^2 + r^2}{4} + \frac{h^2}{3} \right] \qquad I_{33} = m_{\text{fuel}} \left[\frac{R^2 + r^2}{2} \right] \tag{63}$$

$$I'_{11} = I'_{22} = \dot{m}_{\text{fuel}} \left[\frac{r^2}{2} + \frac{h^2}{3} \right] \qquad I'_{33} = \dot{m}_{\text{fuel}}\, r^2 \tag{64}$$

The constant tank's volume model

This model takes into account the variation of the fuel inside considering no variation of the volume off the tank. By looking at Fig. 9a the following equation is found:

$$\left[I_{\text{fuel},\, Tc} \right] = \frac{2}{5}\, m_{\text{fuel}}\, R^2_{\text{tank}} \left[\mathbb{1}_{3\times 3} \right] \qquad \Rightarrow \qquad \left[I_{\text{fuel},\, Tc} \right]' = \frac{2}{5}\, \dot{m}_{\text{fuel}}\, R^2_{\text{tank}} \left[\mathbb{1}_{3\times 3} \right] \tag{65}$$

References

1. Eke, F.O., Mao, T.: On the dynamics of variable mass systems. Int. J. Mech. Eng. Educ. **30**(2), 123–137 (2002)
2. Thomson, W.T.: Equations of motion for the variable mass system. AIAA J. **4**(4), 766–768 (1966)
3. Thorpe, J.F.: On the momentum theorem for a continuous system of variable mass. Am. J. Phys **30**, 637–640 (1962)
4. Grubin, C.: Mechanics of variable mass systems. J. Franklin Inst. **276**(4), 305–312 (1963)
5. Eke, F.O.: Dynamics of Variable Mass Systems, Technical Report NAG2-4003 University of California (1998)
6. Eke, F., Tran, T., Sookgaew, J.: Dynamics of a spinning rocket with internal mass flow. Nonlinear Dynamics and Systems Theory **6**(2), 129–142 (2006)
7. Sookgaew, J., Eke, F.: Effects of substantial mass loss on the attitude motions of a rocket-type variable mass system. Nonlinear Dynamics and Systems Theory **4**(1), 73–88 (2004)
8. Marmureanu, M.I., Fuiorea, I.: Attitude dynamics of a spinning rocket with internal fluid whirling motion. INCAS Bulletin **6**(2), 75 (2014)
9. Meirovitch, L.: General motion of a variable-mass flexible rocket with internal flow. J. Spacecr. Rocket. **7**(2), 186–195 (1970)
10. Reiter, G.S., Thomson, W.T.: Jet damping of a solid rocket-theory and flight results. AIAA J. **3**(3), 413–417 (1965)
11. Murphy, C.H.: Spin jet damping of Rocket-Assisted projectiles. Journal Of Guidance and Control **4**(3), 350–351 (1980)
12. Aslanov, V., Doroshin, A.: The motion of a system of coaxial bodies of variable mass. J. Appl. Math. Mech. **68**(6), 899–908 (2004)
13. Doroshin, A.V.: Analysis of attitude motion evolutions of variable mass gyrostats and coaxial rigid bodies system. Int. J. Non Linear Mech. **45**(2), 193–205 (2010)
14. Quadrelli, M.B., Cameron, J., Balaram, B., Baranwal, M., Bruno, A.: Modeling and simulation of flight dynamics of variable mass systems. In: SPACE Conference and Exposition, San Diego, CA, Paper No. AIAA 2014-4454 (2014)
15. Fox, R.W., McDonald, A.T., Pritchard, P.J.: Introduction to Fluid Mechanics, vol. 7. Wiley, New York (1985)
16. White, F.: Fluid Mechanics. McGraw-Hill Series in Mechanical Engineering. McGraw Hill, New York (2011)
17. Munson, B., Rothmayer, A., Okiishi, T. Fundamentals of Fluid Mechanics, 7th edn. Wiley, Incorporated (2012)

18. Alcorn, J., Schaub, H., Piggott, S., Kubitschek, D.: Simulating attitude actuation options using the basilisk astrodynamics software architecture. In: 67th International Astronautical Congress, Guadalajara, Mexico (2016)
19. Allard, C., Diaz-Ramos, M., Kenneally, P.W., Schaub, H., Piggott, S.: Modular software architecture for fully-coupled spacecraft simulations. In: AAS Guidance and Control Conference, Breckenridge, CO, pp. 593–604. Paper AAS 18-091 (2018)
20. Schaub, H., Junkins, J.L. Analytical Mechanics of Space Systems, 3rd edn. AIAA Education Series, Reston (2014). https://doi.org/10.2514/4.102400